




MACHINE LEARNING-BASED POSITIONING USING MULTIVARIATE TIME SERIES CLASSIFICATION FOR FACTORY ENVIRONMENTS

A PREPRINT

 **Nisal Hemadasa Manikku Badu**
Institute of Telematics
Hamburg University of Technology
21073 Hamburg, Germany
nisal.hemadasa@tuhh.de

 **Marcus Venzke**
Institute of Telematics
Hamburg University of Technology
21073 Hamburg, Germany
venzke@tuhh.de

 **Volker Turau**
Institute of Telematics
Hamburg University of Technology
21073 Hamburg, Germany
turau@tuhh.de

 **Yanqiu Huang**
Faculty of Electrical Engineering
University of Twente
7522NH Enschede, The Netherlands
yanqiu.huang@utwente.nl

August 24, 2023

ABSTRACT

Indoor Positioning Systems (IPS) gained importance in many industrial applications. State-of-the-art solutions heavily rely on external infrastructures and are subject to potential privacy compromises, external information requirements, and assumptions, that make it unfavorable for environments demanding privacy and prolonged functionality. In certain environments deploying supplementary infrastructures for indoor positioning could be infeasible and expensive. Recent developments in machine learning (ML) offer solutions to address these limitations relying only on the data from onboard sensors of IoT devices. However, it is unclear which model fits best considering the resource constraints of IoT devices. This paper presents a machine learning-based indoor positioning system, using motion and ambient sensors, to localize a moving entity in privacy concerned factory environments. The problem is formulated as a multivariate time series classification (MTSC) and a comparative analysis of different machine learning models is conducted in order to address it. We introduce a novel time series dataset emulating the assembly lines of a factory. This dataset is utilized to assess and compare the selected models in terms of accuracy, memory footprint and inference speed. The results illustrate that all evaluated models can achieve accuracies above 80%. CNN-1D shows the most balanced performance, followed by MLP. DT was found to have the lowest memory footprint and inference latency, indicating its potential for a deployment in real-world scenarios.

Keywords Indoor positioning · Machine learning · Sensor fusion · Multivariate time series classification

1 Introduction

Indoor Positioning is a technology widely adopted in many industries, including medical, sales, manufacturing, logistics and construction [5, 19]. It is also among the foremost in technological fronts such as Smart Cities, Industrial Internet of Things (IIoT) [8]. In each of these fields, IPS's play important roles in tracking, navigation, proximity, and inertial measurements [5], thereby injecting more efficiency, accuracy, and safety to processes.

Our work is motivated by insights from animal behavioral scientists. Many animal species possess a natural ability to navigate and recognize their location by utilizing various cues such as geomagnetic fields, celestial bodies, wind

direction, temperature, scent, and visual landmarks. They develop mental maps through learning and memory, enabling them to find routes, recognize environments, and differentiate between different locations. This concept can be applied to the localization of entities following a predetermined path. By processing sensory inputs acquired at a given moment or over a specific time period, an estimation of the current position can be derived. This could be perceived as a sub-problem of Indoor Positioning. However, unlike the conventional indoor localization approaches on determining precise x-y coordinates, we reframe the problem to ascertain a relative segment on a pre-determined path.

A plethora of research efforts addresses the indoor positioning problem from a broad range of approaches. These approaches provide precise x-y coordinates of location estimation. Numerous of these methodologies heavily depend on external infrastructure for reliable and robust functionality, such as in RSSI-based solutions that require consistent signal coverage. However, in the context of applications involving relative positions rather than precise coordinates, such as tracking work-in-progress goods in an assembly line, x-y coordinates bear less significance. Furthermore, deployment of supplementary infrastructure incur additional cost and can be technically unfeasible when considering scenarios such as tunnels or mining sites. Secondly, infrastructure-less systems, like vision-based methods, raise privacy concerns. Thirdly, some approaches rely on external predetermined information and cause accumulated errors, such as a starting point in dead reckoning, which are undesirable in automated processes. Finally, some approaches operate on non-generic assumptions such as Gaussian noise or linear motion dynamics. A more detailed comparison between these existing approaches and our proposed method is contained in subsequent sections.

In order to overcome the aforementioned limitations, this research investigates how indoor positions can be learned from sensor data to enable the execution of the ML model on low power, low performance devices such as micro-controllers. To this end, we leverage a combination of inertial sensors (accelerometer, gyroscope, and magnetometer) and ambient sensors (pressure, temperature, humidity, and spectrum). The recordings from these sensors form multivariate time series, which are fused to derive accurate estimates of an entity’s location along a predefined path. The indoor positioning task is therefore formulated as a Multivariate Time Series Classification (MTSC) problem. Machine learning (ML) is used to extract the underlying information of the sensor data without making any assumptions about noise or motion dynamics, and without relying on prior information to achieve accurate functionality. The challenges arise from the resource-constraint hardware and maintaining precision, especially when environmental conditions are changing.

The addressed problem can be more specifically described using an assembly line in a factory. Assembly lines consist of predetermined routes planned inside the facility to optimize lead time and cost. Goods under work-in-progress that traverse along these routes require tracking in real-time. Modern production lines are digitized and often use enterprise resource planning (ERP) systems. Especially in industry 4.0, monitoring of this process is automated. This requires an asset localization solutions inside highly confidential factory environments complying with strict privacy policies.

To this end, we evaluate the usage of computationally-light ML models such as decision trees (DT) [29], RF [12], which are well suited for severely resource constrained edge devices such as low-end Microcontroller Units (MCUs) with less than 10kB SRAMs [17]. We also choose state-of-the-art of time series classification benchmark architectures as baselines namely, Multilayer Perceptrons (MLP), Convolutional Neural Networks (CNN) [6]. Further, we experiment with the use of more complex Long Short-Term Memory networks (LSTM) in indoor positioning formulated as time series classification [37].

To the best of our knowledge, this work becomes the first of its kind in formulating indoor positioning as an MTSC problem by fusing motion and ambient sensors with no x-y coordinates for particularly relevant environments such as factories, and investigating applicability of potential ML models given the limited hardware constraints, to estimate the relative position. Moreover, state-of-the-art benchmarking Deep Neural Network (DNN) models for Time Series Classification (TSC) [34, 6] are used as baselines for the models formulated in this work, using a novel indoor positioning time series dataset. The contributions of this work can be summarized as follows.

- Motion and ambient sensor measurements are employed to localize a moving entity on a known path consisting of both indoor and outdoor components, with no external infrastructure required. The importance and drawbacks of the sensors are discussed.
- A novel multivariate time series dataset is presented. The dataset contains sensor measurements from IMU, pressure, temperature, humidity and spectrum sensors, collected through traversing three paths.
- The localization problem on a known path is formulated as an MTSC problem. ML models, namely DT, RF, MLP, CNN, LSTM are applied to solve the MTSC. Their performances are compared against the baseline models, based mainly on accuracy, memory footprint, inference latency.

The rest of this paper is organized as follows. The review on the related works is in section 2. Section 3 generalizes the indoor positioning task as an MTSC problem. Section 4 introduces the ML models evaluated in this work. Section 5

describes the novel multivariate time series dataset and a case study for the proposed solution. Section 6 presents the results of evaluations of the formulated ML models and analyses them. Finally, Section 7 provides the conclusion of the work.

2 Related Work

The existing work on indoor positioning [11, 24, 38, 36, 35, 25, 31, 21, 27, 26] can be categorized along three different dimensions: technology-wise, technique-wise and algorithm-wise. Technology-wise solutions branch mainly to satellite-based, radio communication-based, visible light-based, inertial navigation-based, magnetic-based, sound-based and vision-based. The majority of solutions within this available spectrum fail in terms of privacy preservation and independence from external infrastructure, such as setting up wireless access points (APs). Although there exist wireless technology based positioning systems that uphold privacy [14], to the best of our knowledge, all of them require the establishment of supplementary infrastructure within the localization environment. Moreover, certain applications, such as tracking goods in assembly lines, necessitate a relative location of goods rather than precise x-y coordinates. However, to the best of our knowledge, the primary focus of the aforementioned solutions is determining x-y coordinates.

Collaborative use of different technologies also exists (Collaborative Indoor Positioning Systems (CIPS) [26]). Magnetic field-based localization solutions are independent of the external infrastructure and also privacy secured. For most of the localization environments they provide stability, and uniqueness in magnetic signals [4]. They also use fusion of several sensors. However, magnetic based solutions are vulnerable to dynamic environments where electromagnetic disturbances occur such as the motion of metallic structures close to the magnetometer.

Work classified under technique-wise includes dead-reckoning-based, vision analysis-based, triangulation-based, fingerprinting-based and proximity-based. To the best of our knowledge, the latter three techniques require external infrastructure for their operation. Dead-reckoning, to the best of our knowledge, require external information such as initial location and is prone to accumulated error. Vision based systems pose a significant risk to privacy.

Algorithm-wise classification mainly branches to the least square method, maximum likelihood method, deterministic or probabilistic method [26]. Existing fusion-based positioning methods range from conventional methods such as least squares, maximum likelihood, maximum a posterior, and minimum mean squares error, to state estimate methods such as hidden Markov model, Kalman filter, extended Kalman filter, and particle filter, and ML methods such as k-nearest neighbors, random forests (RF), support vector machine, and neural networks [10]. The use cases of ML in this regard have so far been mainly applied to positioning systems based on Received Signal Strength (RSS) and fingerprint [10, 23]. Furthermore, they mainly assume Gaussian noise and linear motion dynamics [23], which may not describe real-world positioning systems.

3 Problem Definition

Indoor positioning is heavily used in asset localization and work-in-progress tracking in production lines, factories and warehousing. The goal is to accurately determine an asset’s location within an enclosed facility as the assets lie stationary or move along predetermined paths. By dividing these paths into smaller segments, the location of the asset, at a given time, can be determined by finding the most likely segment the asset is present in. This can be interpreted as a classification problem. As the asset moves along the path, motion and ambient sensors attached to the asset acquire measurements and record them periodically, in resulting a multivariate time series. This multivariate time series data is then used as inputs to the classification problem on the edge device, on the fly. This problem can be defined in general terms as follows.

Definition 1. *Let P be a path partitioned into l segments, such that $P \rightarrow [s_1, \dots, s_m, \dots, s_l]^T$. For each $m \in \{1, \dots, l\}$ segment s_m is uniquely identified by a label y_m from a set $Y_P = \{y_1, y_2, \dots, y_m, \dots, y_l\}$ of labels of P .*

An asset is being carried along the path P . Neither the speed nor the variation of the speed along the path are known. Further, the times of completion of traversal along the path do not remain constant across several instances of path traversals. Hence, no trivial correlation between asset’s position and the time exists. Further, the path P contains segments along which the asset is carried both on its forward and return journeys, which is analogous to the asset turning around and returning on the same route it took in the forward journey. However, it does not include anomalies such as long pauses while traversing or moving out of the defined path, which could be typically expected in industrial environments such as factories or warehouses.

The following two definitions formally capture the notions of *observation* and *multivariate time series* for paths.

Definition 2. Let X^i denote a univariate time series of a feature i , engineered from the recordings of sensor measurements, as a result of traversing a complete path P . An observation at a given sampling time t is denoted as x_t^i and $X^i = [x_1^i, x_2^i, \dots, x_k^i]^T$, where k is the total number of observations of time series X^i .

Definition 3. Let there be n different features, giving distinct univariate time series for a data-collection run along P . Then, $X = [X^1, X^2, \dots, X^n]$ is then defined as a multivariate time series for P .

Finally we formally define the problem addressed in this work.

Definition 4. Let $X_t = [x_t^1, x_t^2, \dots, x_t^n]$ be the observations of all features in the feature space, at a given time t . The problem addressed in this work is to find a function $f_P^j : \{X_t, X_{t-1}, \dots, X_{t-j}\} \rightarrow Y_P$, that determines the label y_m of the segment in which the object is at time t , using time series $[X_t, X_{t-1}, \dots, X_{t-j}]$, where j is a predetermined window size, such that $j \in \mathbb{Z}_0^+$, and for $j \leq t - 1$ it holds that $f_P^j(X_t, X_{t-1}, \dots, X_{t-j}) = y_m$.

4 Indoor Positioning using DT, RF, CNN and LSTM Networks

In this section, we formulate the architectures of the ML models that we use to learn the function f_P^j defined in definition 4. We use two recently popular time series classification baseline models namely, MLP, and Fully Convolutional Networks (FCN) [6, 34]. Additionally, we use a tree-based approach, namely DT with entropy [28, 30], which is relatively less complex and therefore suitable for use on low-performance edge devices, such as MCUs. We also explore an ensemble approach, namely RF [12, 3]. Lastly, we apply the dataset to vanilla LSTM [13], bidirectional LSTM (BiLSTM), CNN-1D and CNN-2D [18] for solving the time series classification task.

The runtime environment for most existing works related to indoor positioning is a resource-constrained edge device [23]. Therefore, when optimizing ML models, it is not only important to consider the accuracies but also their resource usage. Hence, in this work, we evaluate less complex and lighter models with significant accuracy to fit the problem defined in section 3.

4.1 Decision Trees: DT

In this work, the parameters used for DT are the split criterion (entropy/gini) and the maximum depth (8-22). The best accuracy performance on average is obtained with entropy with a maximum depth of 14, across all three paths. The influence of other hyperparameters such as the minimum sample split and minimum samples leaf, on the accuracy score, is found to be insignificant. Hence maximum tree depth is the only early stopping criteria used. Furthermore, adding more features beyond the most important 17 features does not noticeably improve the model. Consequently, the 17 features mentioned in subsection 5.2 are chosen as input features for all model architectures used in this work.

4.2 Multilayer Perceptrons

A basic MLP is used as a baseline model as proposed by Wang et al. [34]. We fine-tune the model with minor modifications to the hyperparameters to fit our dataset (see Fig 1). An input layer takes 2D inputs with dimensions of (30, 17), (30, 17), and (30, 9) for paths 1, 2, and 3, respectively. Here, 30 denotes the window of timesteps of the time series data taken as inputs, and 17, 17, and 9 are the number of input features of the datasets for paths 1, 2 and 3 respectively. Three hidden fully connected layers with 64 nodes and Rectified Linear Unit (ReLU) [22] activation functions follow. A Flatten layer is included before the output layer with a softmax activation function. Dropouts [32] are omitted as they result in a decrease in training, validation, and test accuracies. Categorical cross entropy is used as the loss function, and the Adam optimization algorithm [16] is used with a learning rate of 0.0003. The batch size is set to 256, and the model is trained over 30 epochs.

4.3 FCN

The proposed FCN architecture by Wang et al. [34] is used as a baseline. Fig. 2 shows our refined FCN architecture. This model has an input layer taking inputs with dimensions of (30, 17, 1), (30, 17, 1), and (30, 9, 1), for paths 1, 2 and 3 respectively. Here, following the same pattern as in the case of MLP, 30 denotes the input sequence length and 17, 17, and 9 are the size of the feature space for paths 1, 2 and 3 respectively. The hidden layers are three distinct convolutional blocks, each containing a 2D convolutional layer (Conv2D), batch normalization layer (BN) [15], ReLU activation layer. The three convolution layers have 16 filters, 2d-kernels of sizes 8, 5 and 3 and stride 1. To avoid overfitting, dropout values of 0.3, 0.3 and 0.2 are added respectively. The convolutional blocks are followed by a 2D global average pooling layer and a Flatten layer. The output dense layer is activated using a softmax activation

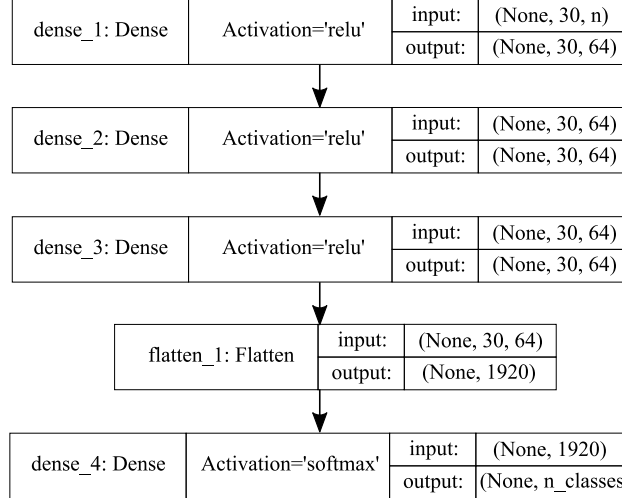


Figure 1: The model architecture of the MLP. n and $n_classes$ represent the number of input features and the number of output classes respectively.

function, and the loss function used is the categorical cross entropy with Adam optimization and a learning rate of 0.00005. The batch size is 100 and the model is trained for 30 epochs.

4.4 Random Forests: RF

The accuracy performance of RF is evaluated across the decision-tree-estimator range from 15 to 35, in multiples of 5. The maximum depth of an estimator is varied within the range from 12 to 16, in the multiples of 2. When the parameters are set below these ranges, the accuracy performance significantly decreases. Above this range, there is no significant improvement in accuracy, however the memory footprint of the models increases drastically. Entropy is maintained as the splitting criterion of all the cases. Considering these factors, maximum depth of 14 is chosen as the optimum, which is equivalent to the best performance achieved using DT, with 25 decision-tree-estimators

4.5 Convolutional Neural Networks: CNN

Using CNN, we optimize two architectures, one using a 1D convolutional layer and the other using a 2D convolutional layer, followed by dense layers in both the cases.

The first CNN model (CNN-1D), similar to MLP, the inputs of dimensions are set to (30, 17), (30, 17), and (30, 9) for paths 1, 2, and 3, respectively. Here, 30 denotes the window of timesteps of the time series data taken as inputs, and 17, 17, and 9 are the number of input features of the datasets for paths 1, 2 and 3 respectively (see Fig. 3). The first layer is a 1D-convolutional layer (Conv1D) with 64 filters and kernel size as 5, activated by a ReLu function. Its output is then passed to a 1D-max pooling layer with pool size 3×3 , stride size 1, with padding set to 'same'. The output is then batch normalized and subsequently passed to a Flatten layer. Then follows two fully connected layers each of size 32, both ReLu-activated. The last is a dense layer, connected fully to the previous dense layers, with a softmax activation function.

In the second model (CNN-2D), input dimensions are (30, 17, 1), (30, 17, 1), and (30, 9, 1) for paths 1, 2, and 3, respectively, where the 3rd dimension with the value 1 refers to the number of channels (see Fig. 4). The first layer consists of a 2D-convolutional layer with 64 filters and kernel size 5×5 , with no padding and is activated by a ReLu. A 2D-max pooling layer is then applied, with pool size 3×3 , stride 1 and padding 'same' type. This is followed by a layer of batch normalization, two fully connected layers both having ReLU activated, a Flatten layer, finally leading to a dense layer with softmax activated.

The categorical cross entropy loss function and Adam optimization with a learning rate of 0.00003 is adopted for both cases above. The model is trained for 30 epochs.

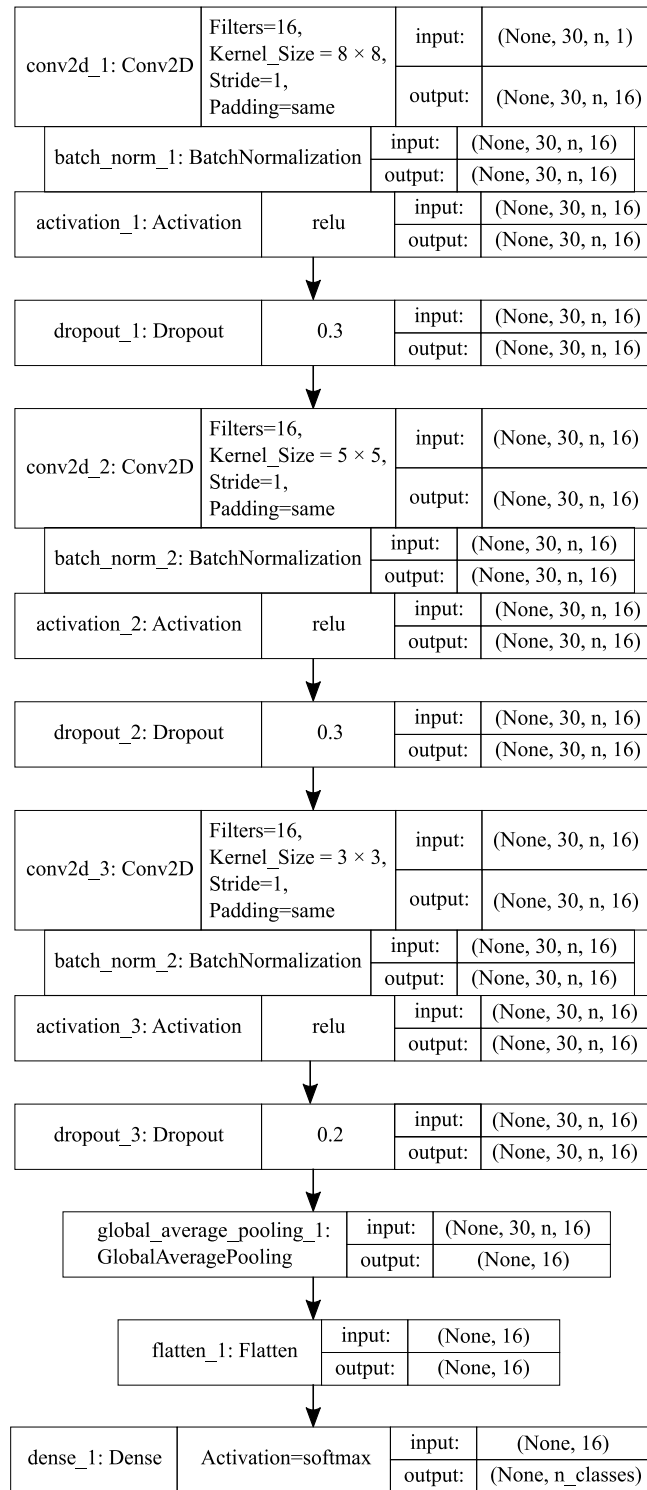


Figure 2: The model architecture of the FCN. n and $n_classes$ represent the number of input features and the number of output classes respectively.

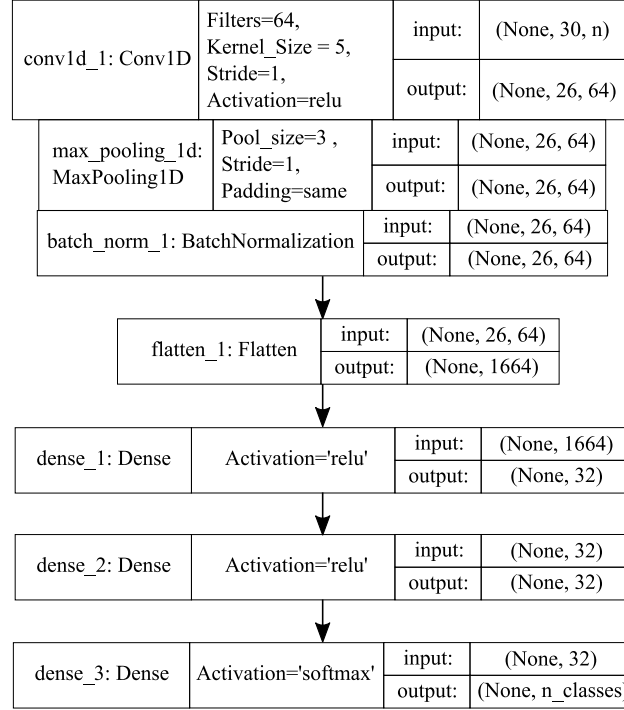


Figure 3: The model architecture of the CNN-1D. n and $n_classes$ represent the number of input features and the number of output classes respectively.

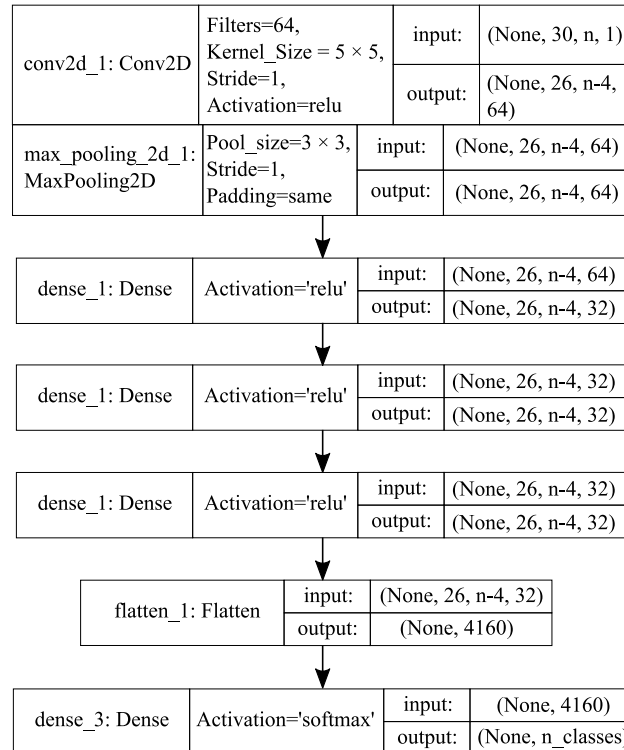


Figure 4: The model architecture of the CNN-2D. n and $n_classes$ represent the number of input features and the number of output classes respectively.

4.6 Long Short-Term Memory networks: LSTM

The Long-Short Term Memory (LSTM) architecture is implemented using an input layer of dimensions (30, 17), (30, 17), and (30, 9) for paths 1, 2, and 3, respectively (see Fig. 5). Three LSTM layers of size 64 each, are connected via 3 dropout layers, each of 0.2, sequentially connecting to a dense layer with a softmax activation function. The categorical cross entropy is selected as the loss function and Adam optimization is employed with a learning rate of 0.00003. The model is trained using batch sizes of 200 for 30 epochs.

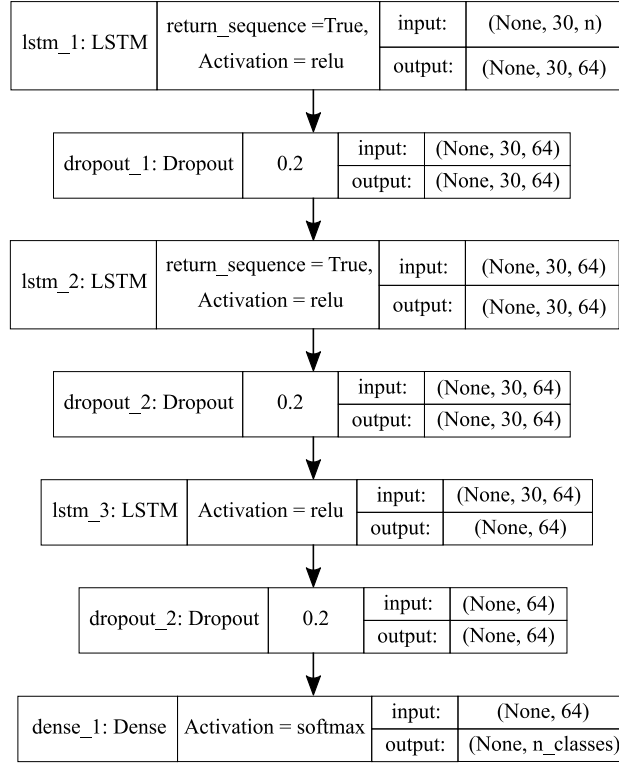


Figure 5: The model architecture of the LSTM. n and $n_classes$ represent the number of input features and the number of output classes respectively.

4.7 Bidirectional Long Short-Term Memory networks: BiLSTM

The proposed bidirectional-LSTM architecture takes inputs with dimensions (30, 17), (30, 17), and (30, 9) for paths 1, 2, and 3, respectively (see Fig. 6). Two BiLSTM layers, each of size 64, are connected via dropouts of 0.3, which leads to the output layer which is activated with a softmax activation function. The categorical cross entropy is used as the loss function and Adam optimization is employed with a learning rate of 0.00003. The model is trained with a batch size of 1024 for 30 epochs.

In the models, the dimensions of the input depend on the time step window size j , and on the feature space size n as described in definition 4 and 3 respectively.

5 Localizing a Moving Object: Motion-Ambient Dataset, Data Preprocessing and Feature Selection

In this section, we describe a use case scenario to verify the claims of this paper. This is done using the *Motion-Ambient* dataset, which is presented for the first time.

We construct a practical scenario, comprising events, that one can expect to have in factories and warehousing, inside the premises of XXX. A moveable data-logging setup is used to collect IMU, pressure, humidity, temperature, and spectrum data across three different paths comprising both indoor and outdoor segments. These paths comprise a variety of dynamics including passages in buildings, elevators, ramps, stairs, terrain with varying roughness such as

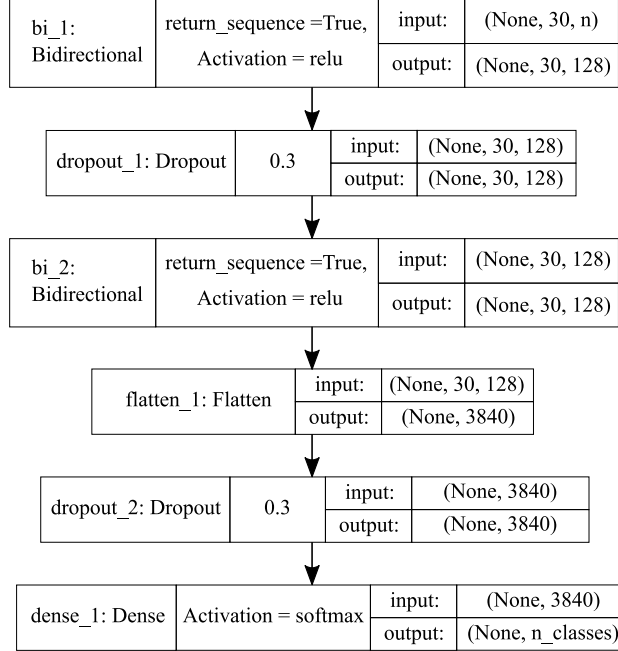


Figure 6: The model architecture of the BiLSTM. n and $n_classes$ represent the number of input features and the number of output classes respectively.

cobblestone, areas with different lighting conditions, magnetic disturbances near metallic structures (e.g. metal door frames), etc., which are commonly encountered in industrial settings. These paths are annotated in real-time with pre-determined segments (or classes) as the setup is being transported.

Motion-Ambient is a time series dataset that is created to benchmark research in indoor localization. In the following subsections, we describe this dataset and its preprocessing steps. Motion-Ambient dataset will be made public including a detailed description, visualizations, analysis and benchmarking of it.

5.1 Dataset Description

The dataset is mainly focused on indoor localization use cases. However, the data-collection-paths pass through indoors spaces, outdoors areas, over diverse terrains, under varying lighting, weather and climatic conditions. The summary of the statistics are given in table 1.

The data-logging-hardware includes two dedicated modules especially designed for this work, based on Raspberry Pi development boards integrated with sensors. These sensor types and their constituent sensor modules are summarized in table 3. Outdoor localization technologies such as GPS and GNSS are not featured among the hardware. Hence they are not features in the dataset. The sampling rate of sensors from the IMU (acceleration, rotation and magnetic flux density) is 24 Hz. The rest of the sensor measurements are sampled at 0.14 Hz. The annotation of the data from Raspberry Pi's are done by connecting a smart phone to it via Bluetooth.

Table 1: Summary of the dataset: data-collection-runs and the samples for each path traversed and the sensors involved

Path	Distance (m)	Runs	Samples	Sensors
1	470	115	1,597,657	IMU measurements, temperature, humidity, pressure, spectrum
2	233	180	1,439,903	IMU measurements, temperature, humidity, pressure, spectrum
3	327	115	1,597,657	IMU measurements

5.2 Dataset Preprocessing

Table 2 shows the dataset before the preprocessing stage. The sensors integrated to the Raspberry Pi have varying and unsynchronized sampling rates. Hence, records are periodically missing in some data columns, especially from the

Table 2: Dataset before preprocessing: t_i and t_j are arbitrary sampling times, where $t_i \neq t_j$. T is the sampling period of IMU sensor. ‘✓’ denotes recorded sensor measurements. ‘-’ indicates that no measurement acquired.

Timestamp	IMU-accelerometer-x	...	IMU-magnetometer-z	temperature	humidity	...
t_i	✓	...	✓	-	-	...
t_{i+T}	✓	...	✓	-	-	...
t_j	-	-	...	✓	✓	...
t_{i+2T}	✓	...	✓	-	-	...

Table 3: Sensors used in the data-logging-hardware and the features extracted from them.

Sensor module	Sensor types	Features extracted
ICM-20948 from TDK	accelerometer	acceleration in x, y, z components [G]
	gyroscope	rotation about x, y, z axes [degrees per second]
	magnetometer	magnetic flux density in x, y, z components [μ T]
BME 688 from Bosch	temperature sensor	temperature[$^{\circ}$ C]
	humidity sensor	humidity [% r.H]
	pressure sensor	pressure [Pa]
AS7341 from AMS	spectrum sensor	yellow, green, blue, indigo, violet [Counts]

ambient sensors with low sampling rate compared to IMU sensors. To deal with these missing values and to match the sampling rates, in our approach we firstly perform backward filling (padding the missing fields with the lastly recorded value) followed by forward filling (padding the missing fields with the next earliest value that is recorded to fill the remaining missing values after backward filling). The resulting data is then applied with a rolling mean filter. The size of the filter is chosen to be marginally greater than the maximum consecutive missing values recorded in that particular column. This operation is performed separately for each column where values are missing. The data is finally min-max normalized, separately for each column. Columns from the resulting dataset-table are selected as features.

5.3 Feature Selection

Out of 7 individual sensors types from 3 sensor modules, 17 measurements are chosen as features. These are given in table 3. The selection is based on the highest feature importance figures in the DT model. This set of features are thereon used for paths 1 and 2 consistently throughout the evaluations using other models described in this work. For path 3, only the 9 IMU sensor measurements are used as features.

6 Results, Analysis and Discussion

In this section, we describe the constraints used in structuring the architectures of the formulated ML models. Furthermore, we introduce the metrics used to evaluate the performance of the models. Based on these metric-scores, we compare, discuss and analyse further insights in detail.

6.1 Description of model architectures and their constraints

Apart from its use in regression problems, the purpose of decision trees is to classify a dataset based on its feature characteristics, while dense layer networks such as MLP can be used for the same tasks, as well as for identifying complex, non-linear patterns in data. RF also used for similar use cases, generally with a higher accuracy and unbiased predictions than decision trees, at the cost of more computations and memory utility. Originally, Convolutional Neural Networks (CNNs) are used to identify spatial patterns in images. However, multivariate time series data can be arranged as a 2D heat map similar to an image. This enables the use of CNNs to capture the local temporal patterns, across time and features. By combining CNNs with dense layers, the aim is to reduce the image patterns learnt into a simple classification problem. Furthermore, CNNs generate large feature spaces. Complex patterns and inter-correlations among these large feature sets can be learnt using the dense layers. Long Short-Term Memory (LSTM) models, on the other hand, learn long-term dependencies between time steps in time series or sequence data. That is, while CNNs are capable of recognizing patterns of a local region of focus of a multivariate time series, LSTMs are capable of learning the relationships between and among several of these regions. In contrast DTs, RFs and MLPs,

compared to LSTMs are not specially designed to extract time correlations of data. However, feeding a time window of data has a positive effect on the accuracy, implying that they are capable of detecting patterns across time, up to an extent.

The presented DT model is optimized after an architecture search with variables namely, split criterion (entropy/gini) and the maximum depth (8-22). The best accuracy performance on average is obtained with entropy, with a maximum depth of 14, across all three paths. The influence of other hyperparameters such as the minimum sample split and minimum samples leaf, on the accuracy score, is found to be insignificant. Hence maximum tree depth is the only early stopping criteria used.

Before selecting the presented architecture of RF, accuracy performance of RF is evaluated across the estimators ranging from 15 to 35, in multiples of 5. The maximum depth of an estimator is varied within the range from 12 to 16, in the multiples of 2. The optimum results are obtained with a maximum depth of 14, with 25 decision-tree-estimators.

We consider MLP and FCN models proposed by Wang et al. (2017) [34] to benchmark the neural network models that we present. Having them as a reference, we experiment with how CNN and LSTM model architectures and their variations to solve the indoor positioning problem. The variation of CNN architecture includes CNN-1D, and CNN-2D, whereas in LSTM, vanilla LSTM (LSTM) and BiLSTM. Hence the architectures of the latter mentioned models are not allowed to vastly deviate from the benchmark models. MLP and FCN models use three blocks of layers in their architecture, except for softmax activated final dense layer. Hence in the variants CNN-1D and LSTM we use architectures with three blocks of layers. An additional dense layer is added of CNN-2D and one BiLSTM layer is taken out from BiLSTM to improve the performance in terms of comparison metrics to an acceptable level compared to benchmark models.

The timestep window size $j = 30$ yields the highest accuracy out of $\{10, 20, 30, 40, 50\}$, for the benchmarking models MLP and FCN. Above this value, the models tend to overfit, and below this value, the models underfit. We use the same timestep window size for all models.

6.2 Accuracy Metrics

In this work, in addition to the accuracy-score used in ML, we use another accuracy metric fine tuned to this specific application called Loc-score.

6.2.1 Accuracy-score

ML classification accuracy-score (accuracy) is the ratio of the number of correct predictions to the total number of predictions, as shown by equation 1. In this work, this is equivalent to the proportion of sensor samples correctly classified with no disparity against annotations that they are assigned.

$$\text{Accuracy-score} = \frac{\text{Total number of correct predictions}}{\text{Total number of predictions}} \quad (1)$$

However, there is no guarantee that the labels used in this work are in 100% agreement with the ground truth, due to labelling noise. This is mainly attributed to the high sampling rates of the sensors which are much larger than average human reaction times, making it difficult to consistently annotate the transitions between segments of a path for all data-collection-runs. To compensate for such inconsistencies in labelling, Grewe introduces the accuracy metric loc-score [9].

Table 4: Accuracy-scores across the ML models. The highest accuracy corresponding to each path is highlighted.

Path	MLP	FCN	Decision Tree	RF	LSTM	BiLSTM	CNN-1D	CNN-2D
1	0.8848	0.8301	0.8394	0.8977	0.8135	0.8445	0.9105	0.8635
2	0.9520	0.9298	0.8405	0.8946	0.8735	0.8872	0.9544	0.8891
3	0.9321	0.9185	0.8777	0.9217	0.9116	0.9013	0.9302	0.8939

6.2.2 Loc-score

Loc-score defines a window of timesteps around transitions from one segment (considered as a class in this problem) to the next, in the true class labels. During the evaluation, predictions to either of the two classes, within this window,

Table 5: Loc-scores across the ML models. The highest loc-score corresponding to each path is highlighted.

Path	MLP	FCN	DT	RF	LSTM	BiLSTM	CNN-1D	CNN-2D
1	0.9079	0.8542	0.8529	0.9199	0.8270	0.8205	0.9315	0.8367
2	0.9660	0.9465	0.854	0.9108	0.8932	0.9058	0.9679	0.9058
3	0.9438	0.9312	0.9033	0.9350	0.9244	0.9164	0.9416	0.9057

are considered correct, while prediction to other classes are considered misclassified. The ratio of the samples consequently correctly predicted and the total number of predictions is defined as the Loc-score. This can be more formally defined as follows.

Definition 5. For a transition from a segment y_m to y_{m+1} , at a given timestep t_{tr} , and a defined window size $2\tau + t_{tr}$, a classification \hat{y}_t , at time t , is considered correct only if $\hat{y}_t \in \{y_m, y_{m+1}\}$, such that $t \in [t_{tr} - \tau, t_{tr} + \tau]$. Then,

$$\text{Loc-score} = \frac{\text{number of correct predictions (per definition)}}{\text{Total number of predictions}}$$

6.2.3 Memory Footprint

The memory footprint of a trained ML model is the amount of memory required to store the network’s parameters, including the network structure, the trained weights and biases of all layers. The higher the memory footprint, the more resources are required by the hardware to deploy the network.

6.2.4 Inference Latency

Inference latency is the time taken for a ML model to make a prediction or classification based on input data.

6.2.5 Throughput

Throughput is defined as the rate of predictions, which in our case is the number of predictions per ms.

Both the inference latency and throughput are measures of how quickly a model can process new data and make accurate predictions.

6.3 Analysis of Results

The results are analysed and discussed in this subsection.

6.3.1 Accuracy

Table 4 and Table 5 demonstrate that the CNN-1D model exhibits the highest accuracy and loc-score numbers for both path 1 and 2. For path 1, CNN-1D is closely followed by the RF and MLP models, respectively. MLP model performs best in terms of accuracy for path 3, followed by the CNN-1D model marginally, and RF with a distinct separation. For path 2, the accuracy value of RF is significantly lower than those of MLP and CNN-1D, and even lower than that of FCN. FCN, BiLSTM, LSTM, and CNN-2D follow thereafter, with their rankings fluctuating for each path. In average, DT has the lowest accuracy, with the exception of path 1.

For $j = 1$, DT and RF both yielded significantly lower accuracy-scores (0.7737, 0.7873, 0.8264 and 0.8216, 0.8722, 0.8583 respectively) and loc-scores (0.7959, 0.7981, 0.8422 and 0.8483, 0.8901, 0.8732 respectively) for paths 1, 2 and 3, compared to when $j = 30$. This demonstrates that tree-based models can capture time correlations to a certain degree, even though they are not tailored for this. Accuracy of DT and RF could be further increased by engineering more optimal features.

In summary, architectures such as MLP, CNN-1D and RF that extract short-to-mid range time dependencies yield higher accuracy figures. The fact that two LSTM variants do not lead to a significant boost in classification accuracy could mean that the dataset does not contain a higher amount of important long-term patterns these models can identify. For paths 2 and 3, the temporal correlation extraction capability of DT is not enough to capture the same amount of feature dynamics as the other models. However, the dataset for path 1 has less complex, more structured data making it easier for both DT and RF to capture. This can be concluded by the relative increment in accuracy metric values for DT and RF in path 1 compared to the other two paths.

CNN-1D demonstrates higher accuracy values than CNN-2D for all three paths. This could be due to architectural changes, such as the addition of batch normalization between layers, which helps regularize the model and improve accuracy in CNN-1D. Additionally, it is possible that Conv1D extracts more features that better represent the data than Conv2D. Conv1D convolves along feature vectors, arranged according to the temporal sequence, which could be more effective at deriving informative features than convolving only a part of the feature space along with their temporal dynamics, all at once.

Despite LSTM and BiLSTM being architectures capable of extracting complex temporal correlations, they do not produce the best results. To understand why, initially, the hyperparameters are varied within the limits of constraints mentioned in subsection 6.1, that is, a maximum of 3 layers with 64 cells in each layer and $j = 30$. This does not improve accuracy. In conclusion, we are left with several reasons such as the dataset having simple temporal complexities, the amount of data required for the models to learn being simply too small, the time step window size $j = 30$ being not large enough, the lesser number of layers results in a too shallow network in the case of BiLSTM, etc., which we do not cover in this paper.

Table 6: Memory footprint of the ML models in MB. The best memory footprint corresponding to each path is highlighted.

Path	MLP	FCN	DT	RF	LSTM	BiLSTM	CNN-1D	CNN-2D
1	7.72	18.72	0.99	24.65	30.92	75.96	5.37	67.00
2	7.63	18.72	0.44	11	30.87	75.74	5.36	66.50
3	7.65	9.93	0.72	17.98	30.88	75.78	5.35	25.65

6.3.2 Memory Footprint

Table 6 shows that, the lowest memory footprint is consumed by the DT, for all three paths. These values are significantly lower than the rest. The highest memory requirement is demanded by the BiLSTM model. For path 3, the memory footprints of the FCN and CNN-2D models are lower than their corresponding versions of paths 1 and 2. This is mainly attributed to the smaller size of the input feature space for path 3 (9), as compared to the other paths (17), since FCN and CNN-2D models depend on the size of the input feature space.

The memory footprint of DT models can be readily accommodated by high-end MCUs such as the ESP32 [33], which has an average of 500kB SRAM and 4MB of flash memory, without further compression, using technologies such as swapping [20]. Pruning of these architectures can reduce their size further, enabling them to be deployed in severely resource-constrained MCUs with minimal loss of accuracy [17]. In edge ML, the device’s size impacts more dominantly than the model architecture, on the energy budget [2]. This can reduce energy consumption and make them suitable for long-term applications, matching well expectations from the industrial positioning applications. Other DNN models can also be deployed on high-end MCUs after optimizing them to fit the resource-constrained hardware [1, 7]. However, this could lead to accuracy compromises.

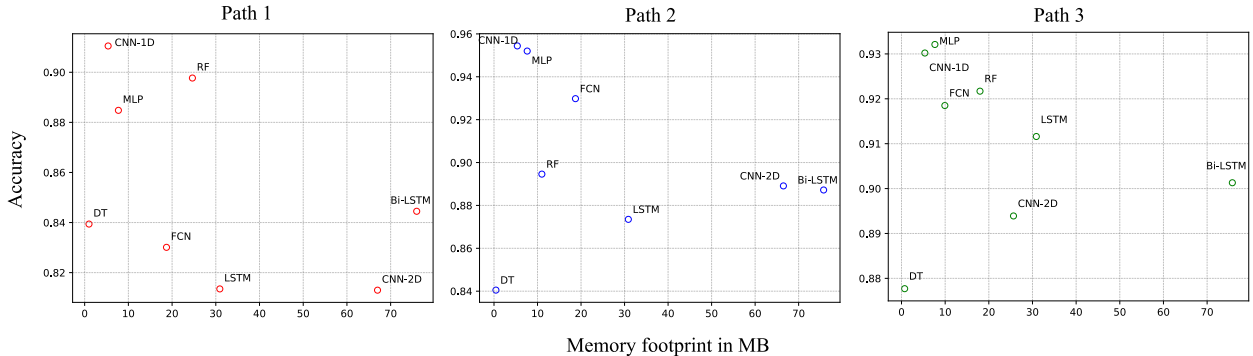


Figure 7: Memory footprint (in MB) against accuracy of the ML models, for all three paths.

6.3.3 Inference Latency and Throughput

In this work inference latency and throughput estimations are performed on an Intel Core i5-10210U CPU at a base clock speed of 1.60 GHz, which has Intel Turbo Boost Technology for increasing the speed up to 2.10 GHz under

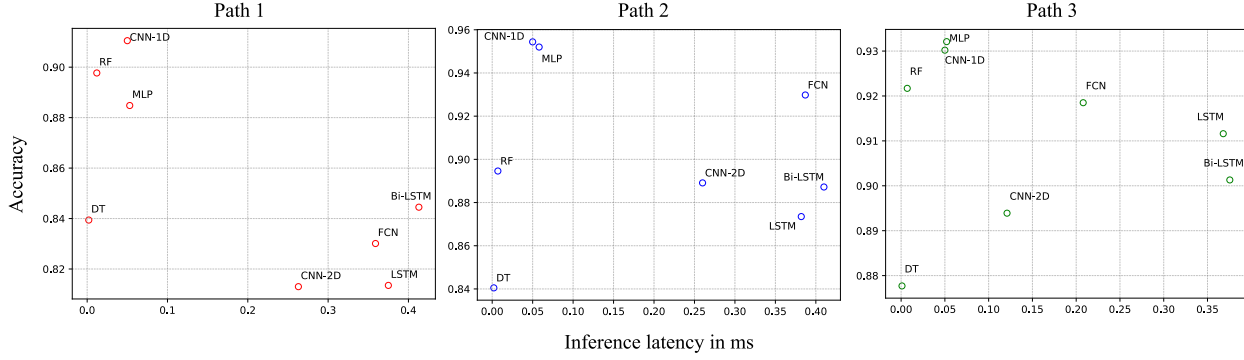


Figure 8: Inference latency (in ms) against accuracy of the ML models, for all three paths.

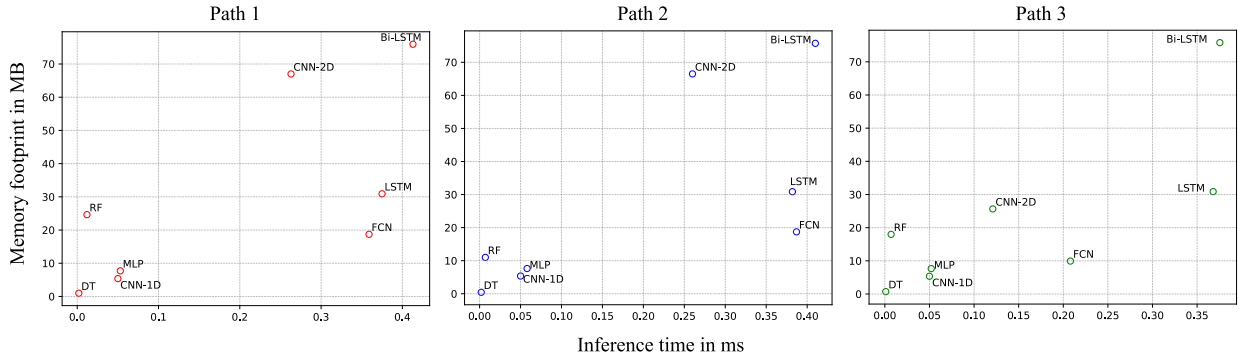


Figure 9: Inference latency (in ms) against memory footprint (in MB) of the ML models, for all three paths.

heavy load. The device is equipped with 16 GB memory and Windows 10 operating system. Hardware with such specifications typically represents the high end of the currently available range of edge devices, in terms of performance. The device is restarted prior to each inference run, and only the inferencing application is allowed to execute in JupyterLab. The size of the dataset for inferencing is maintained at 100,000 for all models tested, i.e., each model is given a batch of 100,000 inputs, with each input having a length of 30 timesteps of input features, for prediction. The total time consumed for this amount of predictions is averaged to get the time per single prediction in milliseconds (ms). Likewise, the test is performed 10 times for each model, and the average and standard deviation are calculated.

Tables 7 and 8 indicate that DT model is the fastest, clearing the other models by a great margin, across all three paths, followed by RF. The next fastest are CNN-1D and MLP models respectively, with a very narrow margin separating each other. CNN-2D model, follows thereafter, succeeded by FCN and LSTM models depicting similar latency performances. BiLSTM model is clearly the slowest compared to the others.

Out of the sensors used in the use case scenario, the IMU sensor is the fastest, sampling data at every 0.041s (~ 24 Hz). All evaluated models are capable of meeting this frequency demand. This, however, is considering the inference latency alone, with the overheads such as feature processing and other processing latencies neglected. MLP, FCN, DT, RF, LSTM, BiLSTM, CNN-1D and CNN-2D can cater to sensor sampling rates up to 14kHz, 2kHz, 5MHz, 172kHz, 2kHz, 2kHz, 18kHz, 3kHz respectively, at their slowest. Considering the application at hand, all these inference rates are faster than the fastest sensor used. Hence, from the inference latency and throughput perspective, using the hardware on which the experiments are run, all the models are deployable in the use case scenario described in this paper.

Apart from the model architectures, the inference latency and throughput substantially depends on the hardware characteristics including the processor speed, memory, operating system if any used, whether any accelerator hardware used and how well the hardware is optimized for deep learning applications.

6.3.4 Correlation between the Metrics

In average, four clusters of models can be identified in terms of memory footprint versus accuracy from figure 7. DTs alone form a cluster having the lowest memory footprint but significantly lower accuracy than the other models for

Table 7: Inference latency (milliseconds) of different ML models with standard deviation, approximated to 3 decimal places (except for DTs). The lowest inference latency for each path is highlighted.

Path	MLP	FCN	DT	RF	LSTM	BiLSTM	CNN-1D	CNN-2D
1	0.053±0.003	0.359±0.012	0.002±0	0.012±0.003	0.375±0.009	0.413±0.028	0.05±0.005	0.263±0.008
2	0.058±0.009	0.387±0.012	0.002±0	0.007±0.001	0.382±0.017	0.41±0.03	0.050±0.001	0.26±0.011
3	0.052±0.010	0.208±0.016	0.001±0	0.007±0	0.368±0.009	0.3755±0.007	0.05±0.005	0.121±0.013

Table 8: Inference throughput of the ML models in predictions per ms, with the standard deviation, approximated to the 2 decimal places. The highest throughput values corresponding to each path is highlighted.

Path	MLP	FCN	DT	RF	LSTM	BiLSTM	CNN-1D	CNN-2D
1	19.03±1.37	2.79±0.09	569.37±77.39	91.09±24.69	2.67±0.07	2.43±0.15	20.29±2.19	3.81±0.11
2	17.46±2.24	2.58±0.08	644.57±35.19	136.45±9.27	2.62±0.11	2.45±0.16	19.92±0.46	3.85±0.16
3	19.98±3.24	4.83±0.37	1080.17±114.97	147.55±8.49	2.72±0.06	2.66±0.05	20.24±1.59	8.37±0.92

paths 2 and 3. CNN-1D and MLP are clustered together, with low memory footprint and high accuracy (high-accuracy-cluster). For all three paths, LSTM consistently represents a cluster with mid-range for both memory footprint and accuracy (mid-range-cluster). For paths 1 and 2, BiLSTM and CNN-2D models form a cluster for paths 1 and 2, having higher memory footprints but lower accuracy than MLP and CNN-1D. For path 3, however, BiLSTM has a significantly higher memory footprint compared to CNN-2D, forming a cluster by its own. CNN-2D in this case joins the mid-range-cluster. RF and FCN mostly represent the high-accuracy cluster, while alternating to mid-range-cluster for path 2 (RF) and path 1 (FCN), respectively.

Figure 8 illustrates inference latency versus accuracy. The models MLP and CNN-1D demonstrate high accuracy and low inference latency consistently in all three paths. The DT and RF models relatively have the lowest latencies, with the latter alternating between high to mid-range accuracies, in contrast to DT which alternate between mid to low range. For paths 1 and 2, the CNN-2D, FCN, LSTM, and BiLSTM models represent a cluster with comparatively higher inference latency, with the majority in mid-range accuracy. The most distinct exceptions is FCN for path 2 which has a higher accuracy. This cluster evolves slightly for path 3 with the FCN and CNN-2D models shifting towards the mid-range latency in contrast to paths 1 and 2.

Memory footprint can be used as an indicator of the scale and complexity of a model. Figure 9, inference latency versus memory footprint, clearly verifies this relationship, which indicates that, as the memory footprint of neural network-based models increases, the inference latency also increases, indicating an increase in model complexity. DT, MLP and CNN-1D models are concentrated at the low memory footprint and low inference latency range. RF models positions itself close to this cluster, but maintaining a notable space from the rest in paths 1 and 3. Models such as FCN, CNN-2D, LSTM, and BiLSTM spread from the mid to high range in terms of both inference latency and memory footprint.

6.4 Discussion and Future Improvements

One of the potential challenges commonly associated with ML-based methods is the occurrence of data drift. This phenomenon can emerge either gradually over time in sensors or due to variations in the positioning environment, such as changes in the factory assembly line setup. In such cases, the models need to be retrained using new data. This highlights a notable drawback of the proposed approaches when compared to the majority of existing IPSs, whose position estimation does not solely rely on ML models. The same limitation holds true in cases when the proposed method requires scaling up.

The generality of the indoor positioning problem addressed in this work, is restricted to the asset’s moving along a predetermined path at randomly varying speeds, with varying times of path completion, and with forward and return journeys lying along the same path. To improve this further, we plan to enhance the models’ capabilities to localize accurately even in the presence of anomalies within the environment. This will involve capturing data instances that encompass various scenarios, including instances where motion deviates from the predefined track exposing the models to unseen data, moments of pause at random locations for varying durations, collisions with nearby structures and other unexpected events. Thereby, we intend to enhance the generality of the presented algorithms.

Furthermore, we intend to expand the generalizability of the evaluated ML models to characterize and classify common motions occurred in indoor environments such as moving along ramps, elevators, conveyor belts, left and right turns, etc. This broadens their applicability on new paths with transfer learning, requiring smaller training datasets,

accelerated training and improved accuracy. From the results, we see MLP and CNN-1D which performs overall the best, consistently for all three paths, are already suitable for this application.

Features such as temperature, humidity, and spectral attributes exhibit seasonality effects that can potentially influence the outcomes of the classification. Nevertheless, our dataset lacks the representation of these seasonal effects. Consequently, the current version of this study does not address accuracy variations across different seasons and will be investigated in future works.

We further plan to investigate the performance of the models by deploying them on low power and low performance edge devices preferably on microcontrollers, while sensing data in real time, on-site.

7 Conclusion

In this paper, we have presented for the first time, an indoor positioning method using ML, by fusing motion and ambient sensors, operating independently from any external infrastructure. We also introduce the novel Motion-Ambient dataset which includes multivariate time series data. Using this dataset, we model the indoor positioning problem as an MTSC problem and formulate, train and evaluate ML models based on the architectures DT, RF, LSTM, BiLSTM, CNN-1D, and CNN-2D. These are compared and analysed against the standard MTSC benchmarking algorithms, MLP and FCN [34] using the comparison metrics, accuracy, loc-score, memory footprint, inference latency and throughput. The results show that all the models achieve accuracies higher than 80%, which is in general sufficiently precise for the type of use cases that we address in this work. All the models meet the latency demands considering the application in hand. The memory footprint however ranges approximately from 0.5 - 76 MB. CNN-1D demonstrates the most balanced performance, closely followed by MLP. It is also worth noting that DT and RF, having the best performance in memory footprint and inference latency, can be made much superior if optimized to enhance accuracy through feature engineering manually. Furthermore, we can conclude that ML can be used to solve the indoor positioning problem. We intend to deploy our system in a real factory environment.

References

- [1] Colby Banbury, Vijay Janapa Reddi, Peter Torelli, Jeremy Holleman, Nat Jeffries, Csaba Kiraly, Pietro Montino, David Kanter, Sebastian Ahmed, Danilo Pau, et al. Mlperf tiny benchmark. *arXiv preprint arXiv:2106.07597*, 2021.
- [2] Colby Banbury, Chuteng Zhou, Igor Fedorov, Ramon Matas, Urmish Thakker, Dibakar Gope, Vijay Janapa Reddi, Matthew Mattina, and Paul Whatmough. Micronets: Neural network architectures for deploying tinyml applications on commodity microcontrollers. *Proceedings of Machine Learning and Systems*, 3:517–532, 2021.
- [3] Leo Breiman. Random forests. *Machine Learning*, 45(1):5–32, 2001. doi:10.1023/a:1010933404324.
- [4] Ting-Hui Chiang, Zao-Hung Sun, Huan-Ruei Shiu, Kate Ching-Ju Lin, and Yu-Chee Tseng. Magnetic field-based localization in factories using neural network with robotic sampling. *IEEE Sensors Journal*, 20(21):13110–13118, 2020. doi:10.1109/JSEN.2020.3003404.
- [5] Pooyan Shams Farahsari, Amirhossein Farahzadi, Javad Rezazadeh, and Alireza Bagheri. A survey on indoor positioning systems for iot-based applications. *IEEE Internet of Things Journal*, 9(10):7680–7699, 2022. doi:10.1109/JIOT.2022.3149048.
- [6] Hassan Ismail Fawaz, Germain Forestier, Jonathan Weber, Lhassane Idoumghar, and Pierre-Alain Muller. Deep learning for time series classification: a review. *Data Mining and Knowledge Discovery*, 33(4):917–963, March 2019. doi:10.1007/s10618-019-00619-1.
- [7] Igor Fedorov, Marko Stamenovic, Carl Jensen, Li-Chia Yang, Ari Mandell, Yiming Gan, Matthew Mattina, and Paul N Whatmough. Tynlstms: Efficient neural speech enhancement for hearing aids. *arXiv preprint arXiv:2005.11138*, 2020.
- [8] Attila Frankó, Gergely Hollósi, Dániel Ficzere, and Pal Varga. Applied machine learning for IIoT and smart production—methods to improve production quality, safety and sustainability. *Sensors*, 22(23):9148, November 2022. doi:10.3390/s22239148.
- [9] Tim Grewe. Smartphone sensor-based locationawareness using decision trees. Master’s thesis, Institute of Telematics, Hamburg University of Technology, 2021.

- [10] Xiansheng Guo, Nirwan Ansari, Fangzi Hu, Yuan Shao, Nkrow Raphael Elikplim, and Lin Li. A survey on fusion-based indoor positioning. *IEEE Communications Surveys & Tutorials*, 22(1):566–594, 2020. doi:10.1109/COMST.2019.2951036.
- [11] S.J. Hayward, K. van Lopik, C. Hinde, and A.A. West. A survey of indoor location technologies, techniques and applications in industry. *Internet of Things*, 20:100608, November 2022. doi:10.1016/j.iot.2022.100608.
- [12] Tin Kam Ho. Random decision forests. In *Proceedings of 3rd International Conference on Document Analysis and Recognition*, volume 1, pages 278–282 vol.1, 1995. doi:10.1109/ICDAR.1995.598994.
- [13] Sepp Hochreiter and Jürgen Schmidhuber. Long short-term memory. *Neural Computation*, 9(8):1735–1780, November 1997. doi:10.1162/neco.1997.9.8.1735.
- [14] Sylvia Holcer, Joaquín Torres-Sospedra, Michael Gould, and Inmaculada Remolar. Privacy in indoor positioning systems: A systematic review. In *2020 International Conference on Localization and GNSS (ICL-GNSS)*, pages 1–6, 2020. doi:10.1109/ICL-GNSS49876.2020.9115496.
- [15] Sergey Ioffe and Christian Szegedy. Batch normalization: Accelerating deep network training by reducing internal covariate shift. In *Proceedings of the 32nd International Conference on International Conference on Machine Learning - Volume 37, ICML'15*, page 448–456. JMLR.org, 2015.
- [16] Diederik P. Kingma and Jimmy Ba. Adam: A method for stochastic optimization, 2014. URL: <https://arxiv.org/abs/1412.6980>, doi:10.48550/ARXIV.1412.6980.
- [17] Ashish Kumar, Saurabh Goyal, and Manik Varma. Resource-efficient machine learning in 2 kb ram for the internet of things. In *Proceedings of the 34th International Conference on Machine Learning - Volume 70, ICML'17*, page 1935–1944. JMLR.org, 2017.
- [18] Yann LeCun, Yoshua Bengio, et al. Convolutional networks for images, speech, and time series. *The handbook of brain theory and neural networks*, 3361(10):1995, 1995.
- [19] Chun Ting Li, Jack C.P. Cheng, and Keyu Chen. Top 10 technologies for indoor positioning on construction sites. *Automation in Construction*, 118:103309, October 2020. doi:10.1016/j.autcon.2020.103309.
- [20] Hongyu Miao and Felix Xiaozhu Lin. Enabling large neural networks on tiny microcontrollers with swapping. *arXiv preprint arXiv:2101.08744*, 2021.
- [21] Sherif Mostafa, Khaled Harras, and Moustafa Youssef. A survey of indoor localization systems in multi-floor environments. August 2022. doi:10.36227/techrxiv.20439648.v1.
- [22] Vinod Nair and Geoffrey E Hinton. Rectified linear units improve restricted boltzmann machines. In *Icml*, 2010.
- [23] Ahasanun Nessa, Bhagawat Adhikari, Fatima Hussain, and Xavier N. Fernando. A survey of machine learning for indoor positioning. *IEEE Access*, 8:214945–214965, 2020. doi:10.1109/access.2020.3039271.
- [24] Huthaifa Obeidat, Wafa Shuaieb, Omar Obeidat, and Raed Abd-Alhameed. A review of indoor localization techniques and wireless technologies. *Wireless Personal Communications*, 119(1):289–327, February 2021. doi:10.1007/s11277-021-08209-5.
- [25] Guanglie Ouyang and Karim Abed-Meraim. A survey of magnetic-field-based indoor localization. *Electronics*, 11(6):864, March 2022. doi:10.3390/electronics11060864.
- [26] Pavel Pascacio, Sven Casteleyn, Joaquín Torres-Sospedra, Elena Simona Lohan, and Jari Nurmi. Collaborative indoor positioning systems: A systematic review. *Sensors*, 21(3):1002, February 2021. doi:10.3390/s21031002.
- [27] Alwin Poulouse, Jihun Kim, and Dong Seog Han. A sensor fusion framework for indoor localization using smartphone sensors and wi-fi RSSI measurements. *Applied Sciences*, 9(20):4379, October 2019. doi:10.3390/app9204379.
- [28] J. R. Quinlan. Induction of decision trees. *Machine Learning*, 1(1):81–106, March 1986. doi:10.1007/bf00116251.
- [29] J. Ross Quinlan. Induction of decision trees. *Machine learning*, 1(1):81–106, 1986.
- [30] Steven L. Salzberg. C4.5: Programs for machine learning by j. ross quinlan. morgan kaufmann publishers, inc., 1993. *Machine Learning*, 16(3):235–240, September 1994. doi:10.1007/bf00993309.
- [31] Andrey Sesyuk, Stelios Ioannou, and Marios Raspopoulos. A survey of 3d indoor localization systems and technologies. *Sensors*, 22(23):9380, December 2022. doi:10.3390/s22239380.

- [32] Nitish Srivastava, Geoffrey Hinton, Alex Krizhevsky, Ilya Sutskever, and Ruslan Salakhutdinov. Dropout: a simple way to prevent neural networks from overfitting. *The journal of machine learning research*, 15(1):1929–1958, 2014.
- [33] Espressif Systems. Esp32 series - espressif systems. URL: <https://www.espressif.com/en/products/socs>.
- [34] Zhiguang Wang, Weizhong Yan, and Tim Oates. Time series classification from scratch with deep neural networks: A strong baseline, 2016. URL: <https://arxiv.org/abs/1611.06455>, doi:10.48550/ARXIV.1611.06455.
- [35] Yuan Wu, Hai-Bing Zhu, Qing-Xiu Du, and Shu-Ming Tang. A survey of the research status of pedestrian dead reckoning systems based on inertial sensors. *International Journal of Automation and Computing*, 16(1):65–83, September 2018. doi:10.1007/s11633-018-1150-y.
- [36] Tian Yang, Adnane Cabani, and Houcine Chafouk. A survey of recent indoor localization scenarios and methodologies. *Sensors*, 21(23):8086, December 2021. doi:10.3390/s21238086.
- [37] Wennian Yu, Il Yong Kim, and Chris Mechefske. Analysis of different RNN autoencoder variants for time series classification and machine prognostics. *Mechanical Systems and Signal Processing*, 149:107322, February 2021. doi:10.1016/j.ymssp.2020.107322.
- [38] Faheem Zafari, Athanasios Gkelias, and Kin K. Leung. A survey of indoor localization systems and technologies. *IEEE Communications Surveys & Tutorials*, 21(3):2568–2599, 2019. doi:10.1109/COMST.2019.2911558.